XLVI CILAMCE
VITÓRIA - ES - BRAZIL - 2025
XLVI IBERO-LATIN AMERICAN CONGRESS ON COMPUTATIONAL METHODS IN ENGENEERING

Constitutive Simulation of Synthetic Fibers for Offshore Mooring Under Cyclic Loading: Hysteresis Stabilization and Stiffness Evolution

Daniel M. da Cruz[1,2], Larissa B. Zangalli[2], Aleones J. da Cruz Junior[3], Ana Lucia N. da Silva[4,5], Ivan N. Bastos[6], Carlos Eduardo M. Guilherme[7], Fernanda M. Clain[7], Jakson M. Vassoler[1], Felipe T. Stumpf[1]

[1]*Graduate Program in Mechanical Engineering, Federal University of Rio Grande do Sul*
Sarmento Leite St., 425, 90050-170, Porto Alegre/RS, Brazil
daniel.cruz@ufrgs.br, jmvassoler@ufrgs.br, felipe.stumpf@ufrgs.br
[2]*Tecnofibers Desenvolvimento e Tecnologia Ltda.*
Doutor Hermes Atilio Mariani St., 438, 88308-030, Itajaí/SC, Brazil
larissa@tecnofibers.com
[3]*Federal Institute of Education, Science and Technology Goiano*
Wilton Monteiro da Rocha Ave, 75389-269, Trindade/GO, Brazil
aleones.junior@ifgoiano.edu.br
[4]*Institute of Macromolecules Professor Eloisa Mano, Federal University of Rio de Janeiro*
Horácio Macedo Ave, 2030, 21941-598, Rio de Janeiro/RJ, Brazil
ananazareth@ima.ufrj.br
[5]*Environmental Engineering Program, Federal University of Rio de Janeiro*
Athos da Silveira Ramos Ave, 149, 21941-909, Rio de Janeiro/RJ, Brazil
[6]*Polytechnic Institute, Rio de Janeiro State University*
Rua Bonfim St., 25, 28625-570, Nova Friburgo/RJ, Brazil
inbastos@iprj.uerj.br
[7]*School of Engineering, Federal University of Rio Grande*
Itália Ave, km8, 96203-000, Rio Grande/RS, Brazil
carlosguilherme@furg.br, fernandaclain@furg.br

Abstract. This study presents a constitutive numerical simulation framework for modeling the cyclic mechanical behavior of synthetic fibers under repeated tensile loading, with a particular focus on hysteresis stabilization and stiffness evolution. The simulation approach is based on finite strain elasticity theory and employs a phenomenological strain energy function (Modified Yeoh model) calibrated with experimental data. Two types of fibers commonly used in offshore mooring systems, high-modulus polyethylene (HMPE) and polyester (PET), were investigated at the multifilament level. Experimental tests consisted of sinusoidal zero-to-tension load cycles up to 45% of the Yarn Break Load (YBL), with a frequency of 0.1 Hz, and extended to 100 cycles. Numerical simulations were conducted for selected cycles (1st, 25th, 50th, 75th, and 100th), and their convergence was evaluated using average relative error. Results indicate that simulation accuracy improves with hysteresis stabilization, especially after initial inelastic effects diminish. A correlation was observed between normalized stiffness and numerical convergence, suggesting that stiffness stabilization may serve as an indicator of model reliability. These findings support future extensions to other structural levels and testing protocols, contributing to the advancement of predictive modeling in offshore fiber applications.

Keywords: Numeric assessment, Mechanical properties, Dynamic load, Continuum mechanics, Strain energy function

1 Introduction

Synthetic fibers have played an increasingly important role in engineering applications, particularly in structural systems that require high specific strength, flexibility, low weight, and resistance to environmental degradation [1]. In the offshore sector, these materials have become fundamental components in mooring lines, gradually replacing traditional steel catenary systems and enabling more efficient configurations, such as synthetic taut-leg moorings [2–5]. Among the most widely used fibers, polyester (PET) stands out for its mechanical robustness, en-

vironmental stability, and competitive cost, having been the primary industrial choice for mooring applications for decades. In parallel, high-performance fibers such as high-modulus polyethylene (HMPE) have gained prominence in applications that demand higher tenacity, lower density, and buoyancy [6–10].

Despite experimental advances and the extensive characterization of the physical and mechanical properties of these fibers, the challenge of accurately understanding and simulating their nonlinear behavior under cyclic loading conditions remains. In particular, the mechanical response under repeated loading often involves complex phenomena such as hysteresis stabilization, accumulation of residual strains, and stiffness evolution throughout the cycles [11, 12]. These aspects are critical for the reliable modeling of the structural performance of fibers in offshore operations, where cyclic load variations are constant and unavoidable.

In this context, the present work proposes a constitutive numerical approach based on a phenomenological hyperelastic formulation, employing a modified Yeoh strain energy function coupled with a parametric optimization routine built upon the principles of continuum mechanics. The modeling is carried out in tensorial terms, using the decomposition of the deformation gradient and the explicit definition of stress and strain tensors, enabling a consistent representation of the constitutive behavior across different deformation regimes.

The model calibration is performed using experimental data obtained from dynamic cyclic tensile tests conducted on PET and HMPE multifilaments, with load amplitudes ranging from 0 to 45% of the Yarn Break Load (YBL), at a frequency of 0.1 Hz and totaling 100 cycles. The 1st, 25th, 50th, 75th, and 100th cycles were selected as references for numerical calibration, in order to capture both the initial hysteresis effects and the subsequent stabilization and evolution of the mechanical behavior over time.

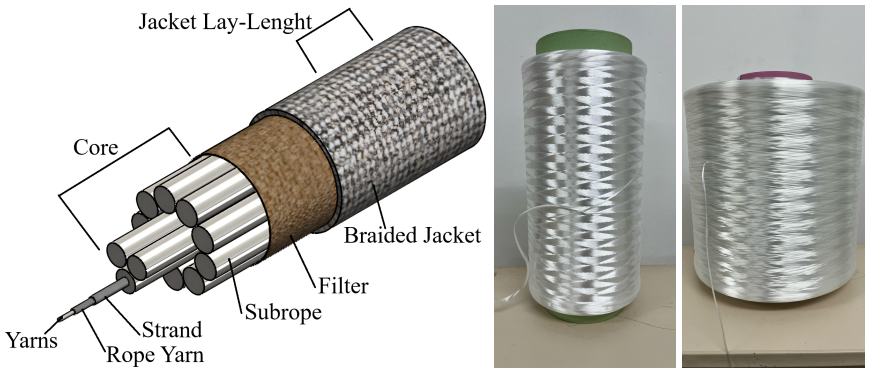
This study is part of a well-established research line that investigates the constitutive numerical response of synthetic fibers based on phenomenological models calibrated with experimental data. Previous works have addressed various fiber types, hybrid configurations, distinct mechanical behaviors, and different construction levels [13–18]. Although the numerical code has been employed in the aforementioned studies by the research group, the present work is pioneering in applying this tool to the simulation of hysteresis stabilization under repeated cyclic loading in PET and HMPE fibers, including the assessment of the model's validity under both initial and stabilized conditions.

Thus, the central objective of this work is to develop and validate a constitutive simulation framework capable of representing the cyclic mechanical response of synthetic fibers subjected to repeated dynamic loading, with emphasis on hysteresis stabilization and gradual stiffness evolution. The ultimate goal is to provide a solid foundation for incorporating these fibers into more realistic offshore system simulations, thereby enhancing the predictive capabilities of numerical tools applied to the design of synthetic mooring systems and advancing both the multiscale understanding of these materials and the numerical modeling approaches used in ocean engineering.

2 Materials and Methods

2.1 Fiber Information and Mechanical Test

The fibers under investigation are high-modulus polyethylene (HMPE) and polyester (polyethylene terephthalate, PET), both in the form of multifilaments (or yarns), which represent the basic structural unit for manufacturing offshore mooring ropes (Fig. 1a). The samples were extracted from a virgin spool of untwisted multifilament (Fig. 1b and Fig. 1c). Initial characterization tests were conducted on the synthetic fibers, including linear density, Yarn Break Load (YBL), and linear tenacity.



(a) Mooring rope schematic levels [19] (b) HMPE spool (c) PET spool

Figure 1. Synthetic fibers samples.

Table 1 presents the results obtained from the initial characterization (linear density, break load, linear tenacity), as well as the specific mass (ρ) and specific cost of the fibers.

Table 1. Results for initial mechanical characterization and information.

Property/information	HMPE	PET
Linear density [tex] or [g/km]	181.20	227.30
Break force, YBL [N]	560.73	182.47
Break strain [%]	2.98	13.23
Break stress [MPa]	3001.70	1107.82
Linear tenacity [N/tex]	3.095	0.803
Specific mass [g/cm^3]	0.97	1.38
Specific cost [US/kg]	19.50	3.80

For the stress values shown in Table 1, the conventional mathematical definition of force over area is difficult to apply due to the lack of precision in determining the cross-sectional area of a yarn bundle. Therefore, an alternative mathematical formulation is adopted, where the stress (σ) is calculated based on the breaking force (F), the linear density (ρ_L), and the specific mass (ρ) of the material, as defined in eq. (1):

$$\sigma[\text{MPa}] = \frac{F[\text{N}] \times \rho[\text{g/cm}^3]}{\rho_L[\text{g/m}]}. \tag{1}$$

The dynamic loading cycles to be simulated numerically and calibrated against experimental measurements consist of zero-to-tension sinusoidal loadings at a frequency of 0.1 Hz, load-controlled, with amplitudes ranging from 0 to 45% of the YBL, totaling 100 cycles. The tests were conducted for both fiber types using an Instron ElectroPuls E3000 dynamic testing machine. Based on the collected data, the corresponding numerical simulations were carried out for a set of five cycles per fiber: the 1st, 25th, 50th, 75th, and 100th cycles.

All tests (initial characterization and dynamic loading) were performed under controlled temperature and humidity conditions in accordance with ISO 139 [20].

2.2 Numeric Code Description

The numerical simulations in this study are based on the continuum mechanics framework for finite deformations, following Simo and Hughes [21] development. The implementation was developed in MATLAB, and the material behavior is described using hyperelastic theory with a phenomenological strain energy function.

Let $\Omega \subset \mathbb{R}^3$ be a deformable body subjected to a finite deformation $\varphi : \Omega \to \mathbb{R}^3$, with deformation gradient $\mathbf{F} = \partial\varphi(\mathbf{X})/\partial\mathbf{X}$ and Jacobian $J = \det \mathbf{F} > 0$. The deformation is split multiplicatively into a volumetric ($\hat{\mathbf{F}}$) and an isochoric ($\bar{\mathbf{F}}$) part as $\mathbf{F} = J^{1/3}\,\mathbf{I}\,J^{-1/3}\mathbf{F} = \hat{\mathbf{F}}\,\bar{\mathbf{F}}$, following the Flory decomposition [22].

For nearly incompressible polymeric materials, only the isochoric contribution of the strain energy function is considered, i.e., $W = W^{\text{iso}}(\bar{\mathbf{C}})$, where $\bar{\mathbf{C}} = \bar{\mathbf{F}}^T\bar{\mathbf{F}} = J^{-2/3}\mathbf{C}$ is the isochoric right Cauchy-Green deformation tensor. The relevant invariants used in the model are derived from $\bar{\mathbf{C}}$ (isochoric contribution), with $\bar{I}_1 = \text{tr}(\bar{\mathbf{C}})$ and $\bar{I}_2 = \frac{1}{2}[(\text{tr}(\bar{\mathbf{C}}))^2 - \text{tr}(\bar{\mathbf{C}}^2)]$. For incompressible materials, $\bar{I}_3 = \det(\bar{\mathbf{C}}) = 1$.

The constitutive model introduces an internal variable $\mathbf{H}$ to capture viscoelastic memory effects, updated at each time step (Δt_n) as a function of the material relaxation (τ_i) and the Piola-Kirchhoff stress in isochoric term ($\bar{\mathbf{S}}$), shown in eq. (2):

$$\mathbf{H}_{n+1} = e^{-\Delta t_n/\tau_i}\,\mathbf{H}_n + e^{-\Delta t_n/(2\tau_i)}\left(\bar{\mathbf{S}}_{n+1} - \bar{\mathbf{S}}_n\right). \tag{2}$$

This stress tensor in isochoric terms ($\bar{\mathbf{S}}$) is also presented in eq. (3):

$$\bar{\mathbf{S}} = 2\left[\frac{\partial W}{\partial I_1} + \frac{\partial W}{\partial I_2}\right]\mathbf{I} - 2\,\frac{\partial W}{\partial I_2}\,\bar{\mathbf{C}} + 2\,\frac{\partial W}{\partial I_3}\,I_3\,\bar{\mathbf{C}}^{-1}. \tag{3}$$

Deviatoric functions are applied to both stress and internal variable tensors to isolate the isochoric contributions (superscript with "$\circ$" indicates the execution of a deviatoric function), and thus the final stress tensor is computed (where γ is a parameter which corresponds to a stiffness portion of the model), as shown eq. (4):

$$\mathbf{S}_{\text{final}} = (\gamma - 1)\,\mathbf{S}^{\circ}_{n+1} + \gamma\,\mathbf{H}^{\circ}_{n+1}. \tag{4}$$

To obtain the spatial stress tensor for comparison with experimental data, a push-forward operation is applied to yield the Kirchhoff stress, eq. (5):

$$\boldsymbol{\sigma}_{n+1} = \mathbf{F}_{n+1}\, \mathbf{S}_{\text{final}}\, \mathbf{F}_{n+1}^{T}. \tag{5}$$

Model performance is assessed by computing the mean relative error between experimental (σ_{exp}) and numerical (σ_{num}) stress values, as indicated in eq. (6):

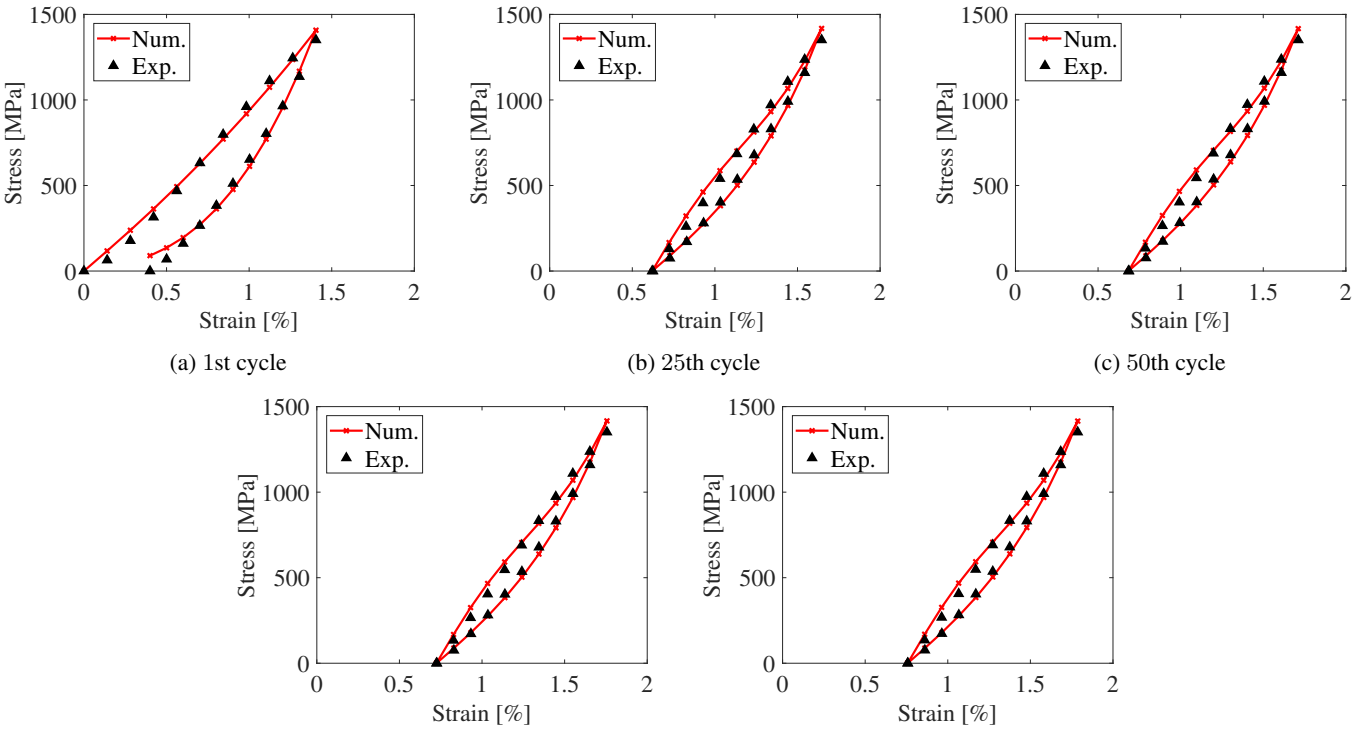
$$\epsilon\,[\%] = \frac{1}{n}\sum_{i=1}^{n}\left|\frac{\sigma_{\text{exp}_i} - \sigma_{\text{num}_i}}{\sigma_{\text{exp}_i}}\right| \times 100. \tag{6}$$

In eq. (3), note that the strain energy function (W) is employed. In this case, Modified Yeoh model is used [23]. This phenomenological formulation was chosen due to its proven ability to minimize numerical error in cyclic simulations involving synthetic fibers [13]. The Modified Yeoh model is defined according eq. (7):

$$W = C_1(I_1 - 3) + C_2(I_1 - 3)^2 + C_3(I_1 - 3)^3 + \frac{C_4}{C_5}\left[1 - \exp\left(-C_5(I_1 - 3)\right)\right]. \tag{7}$$

3 Results and Discussion

The graphical results of the numerical simulations are presented together with the respective selected cycles in Fig. 2 for HMPE and Fig. 3 for PET. In addition to the numerical simulations, all plots include the discrete experimental data points used for calibration. Table 2 presents the mathematical criterion of the mean error (ϵ) for each simulation, calculated according to eq. (6).



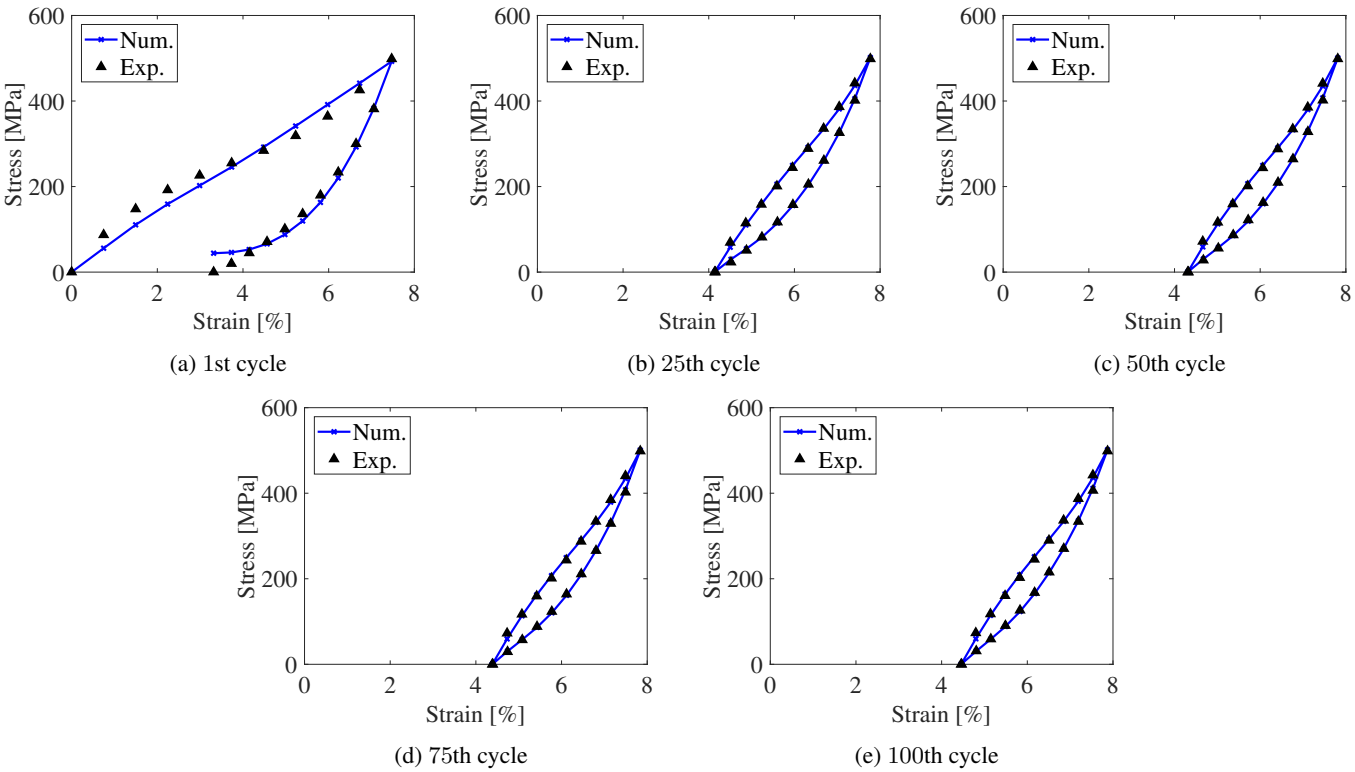
(a) 1st cycle (b) 25th cycle (c) 50th cycle

(d) 75th cycle (e) 100th cycle

Figure 2. Graphical results of constitutive numerical simulations for the HMPE.

Table 2. Results of the mean errors of the constitutive numerical simulations, in percentage.

Cycle	1st	25st	50st	75st	100st
HMPE	15.093	7.322	6.918	6.875	6.692
PET	15.711	3.517	2.630	2.577	2.207



(a) 1st cycle (b) 25th cycle (c) 50th cycle

(d) 75th cycle (e) 100th cycle

Figure 3. Graphical results of constitutive numerical simulations for the PET.

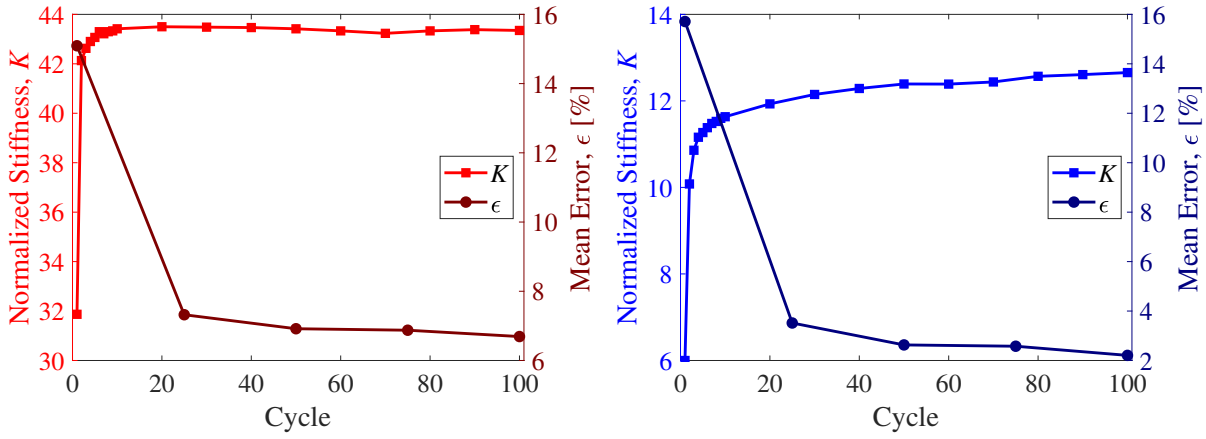
In the presented graphical results, it is evident that the simulations for the 1st cycle in both materials (Fig. 2a and Fig. 3a) exhibit low convergence, which can be attributed to the inelastic components still present in the fibers at the onset of dynamic cycling. When analyzing the subsequent cycles for each fiber, the graphical criterion indicates a well-defined stabilization by the 25th cycle, with little variation in mechanical behavior or in the quality of the numerical simulation compared to the hundredth (and final) cycle. Based on the mathematical mean error criterion (ϵ), a progressive improvement in the convergence of the numerical simulation is observed with increasing cycle count, yielding the lowest mean errors for the 100th cycle.

Still in Fig. 2 and Fig. 3, a significant effect can be observed regarding the inelastic components. At the end of the 1st cycle for HMPE (Fig. 2a), the strain at the end of the cycle is $\approx 0.4\%$, whereas at the end of the 100th cycle (Fig. 2e) it reaches $\approx 0.75\%$, that is, the strain of the first cycle corresponds to $\approx 53\%$ of the final strain of the dynamic test for HMPE. For polyester, at the end of the 1st cycle (Fig. 3a), the final strain is $\approx 3.3\%$, and at the end of the 100th cycle (Fig. 3e) it is $\approx 4.5\%$, meaning that the first cycle corresponds to $\approx 73\%$ of the final strain of the dynamic test for PET. This behavior suggests that PET exhibits a more pronounced initial accommodation, rapidly consuming most of the inelastic strain. As a consequence, the stabilization of the cyclic responses occurs more efficiently in this material, which is reflected in the lower mean errors for PET when compared to HMPE, as observed in the higher-order cycles (Table 2).

It should also be noted, in Table 2, specifically in the comparison between the 75th and 100th cycles, that PET exhibits a significant reduction in mean error ($\approx 15\%$), whereas HMPE shows a considerably smaller mean error reduction between these simulations ($\approx 3\%$).

Based on the experimental data, the normalized stiffness (K) of each cycle can be calculated using the expression $K = (\Delta F/YBL) \,/\, (\Delta L/L_0)$. It is important to note that, regardless of whether force or stress is used, the numerator represents the load variation in the dynamic cycling, which is fixed at 0.45, while the denominator corresponds to the strain variation $\Delta\varepsilon$ that occurs within each cycle. Accordingly, Fig. 4 presents the experimentally obtained normalized stiffness values for each material, plotted alongside the mean errors from the numerical simulations, in Fig. 4a for HMPE and Fig. 4b for PET.

It can be observed in Fig. 4 that the regions with lower error coincide with those where the normalized stiffness stabilizes. Although it cannot be stated that a specific stiffness value directly ensures good convergence of the constitutive numerical simulation under mechanical hysteresis, the observed trend should be taken into account. An important distinction must be highlighted in the data: while the numerical simulations are performed for five equally spaced cycles, the normalized stiffness values are calculated from experimental data collected at 19 points, organized in progression by magnitude (unit-based within the tens, and tens-based within the hundreds).



(a) HMPE (b) PET

Figure 4. Results of normalized stiffness and mean simulation error in different cycles in dynamic loading.

Therefore, normalized stiffness should be regarded as an important criterion for the convergence of constitutive numerical simulations. If the objective is to perform a numerical simulation to obtain a strain energy model that represents the constitutive behavior under loading and unloading conditions, normalized stiffness (particularly its stabilization), serves as a strong indicator of the model's capability to accurately capture such behavior. This is closely related to the viscoelasticity and the progressive removal of inelastic contributions over successive cycles.

In Fig. 4, considering the region where normalized stiffness stabilizes and the region where the numerical simulation error also stabilizes, it is possible to establish a mathematical inverse relationship that allows one variable to be "predicted" based on the other. Naturally, several caveats apply to the validity of this relationship, primarily due to the specificity of the testing conditions. Such a correlation can only be considered valid under the parameters evaluated: multifilament level, zero-to-tension loading, cycling from 0 to 45% of the YBL, and the use of high-modulus polyethylene and polyester fibers. Under different conditions, this relationship is likely to change.

4 Conclusion

This study presented a constitutive numerical simulation framework to represent the cyclic behavior of synthetic fibers subjected to repeated tensile loading, focusing on the stabilization of mechanical hysteresis and the evolution of stiffness. The proposed model, based on finite strain elasticity theory and a modified Yeoh strain energy function, demonstrated a strong ability to reproduce the experimental response of PET and HMPE fibers, especially from the intermediate cycles onward, where initial inelastic effects become less significant.

The combined analysis of experimental data and simulations revealed that normalized stiffness tends to stabilize over the loading cycles, a behavior that directly correlates with the progressive improvement in numerical convergence. This correlation suggests that normalized stiffness may serve as an indicative parameter for both stabilization and fitting quality in constitutive modeling under cyclic behavior.

As future research perspectives, it is proposed to deepen the understanding of the relationship between stiffness and numerical performance, through the empirical equations and the validation of these relationships under different testing protocols. Furthermore, investigating the sensitivity of the model parameters to variations in experimental data is relevant for expanding the understanding of the model's robustness and adaptability.

Other extensions of this study include applying the proposed approach to different structural levels, such as twisted legs and subropes, as well as expanding the experimental scope to include load cycles with varying amplitudes, frequencies, and preloading regimes. These advancements are expected to contribute to the consolidation of a comprehensive database that enables the use of neural networks or machine learning techniques to achieve accurate predictions of the constitutive behavior, based on phenomenological models with low computational cost.

Acknowledgements. We thank for the financial support to the company Tecnofibers Desenvolvimento e Tecnologia LTDA. This study was financed in part by the CAPES, finance code 001, besides CNPq, grant number 307889/2022. We would also like to thank FAPERJ, FAPERGS, and Finep.

Authorship statement. The authors hereby confirm that they are the sole liable persons responsible for the authorship of this work, and that all material that has been herein included as part of the present paper is either the property (and authorship) of the authors, or has the permission of the owners to be included here.

References

[1] G. Bhat, ed. *Structure and Properties of High-Performance Fibers*. Woodhead Publishing Series in Textiles. Woodhead Publishing, 2017.
[2] C. J. M. Del Vecchio. *Light weight materials for deep water moorings*. PhD thesis, University of Reading, Reading, UK, 1992.
[3] S. Banfield and N. Casey. Evaluation of fibre rope properties for offshore mooring. *Ocean Engineering*, vol. 25, n. 10, pp. 861–879, 1998.
[4] P. Davies, M. François, F. Grosjean, P. Baron, K. Salomon, and D. Trassoudaine. Synthetic mooring lines for depths to 3000 meters. In *Offshore Technology Conference*, pp. OTC–14246–MS, Houston, Texas, USA, 2002.
[5] J. G. Williams, A. Miyase, D. Li, and S. S. Wang. Small-scale testing of damaged synthetic fiber mooring ropes. In *Offshore Technology Conference*, pp. OTC–14308–MS, Houston, Texas, USA, 2002.
[6] M. B. Bastos. Improved high tenacity/high modulus polyester for stiffer mooring ropes. In *2013 MTS/IEEE OCEANS - Bergen*, pp. 1–5, Bergen, Norway, 2013.
[7] S. D. Weller, L. Johanning, P. Davies, and S. J. Banfield. Synthetic mooring ropes for marine renewable energy applications. *Renewable Energy*, vol. 83, pp. 1268–1278, 2015.
[8] M. B. Bastos, E. B. Fernandes, and A. L. N. da Silva. Performance fibers for deep water offshore mooring ropes: Evaluation and analysis. In *OCEANS 2016 - Shanghai*, Shanghai, China, 2016.
[9] M. B. Bastos and A. L. N. da Silva. Evaluating offshore rope fibers: Impact on mooring systems integrity and performance. In *Offshore Technology Conference*, pp. OTC–30830–MS, Houston, Texas, USA, 2020.
[10] D. M. da Cruz, L. B. Zangalli, M. A. Barreto, A. L. N. da Silva, and I. N. Bastos. Offshore mooring challenges for FOWT systems and MRE devices: Synthetic fiber solutions for mooring ropes. In *ROG.e 2024*, pp. 3210, Rio de Janeiro, Brasil, 2024a.
[11] H. Liu, W. Huang, Y. Lian, and L. Li. An experimental investigation on nonlinear behaviors of synthetic fiber ropes for deepwater moorings under cyclic loading. *Applied Ocean Research*, vol. 45, pp. 22–32, 2014.
[12] S. Xu, S. Wang, H. Liu, Y. Zhang, L. Li, and C. Guedes Soares. Experimental evaluation of the dynamic stiffness of synthetic fibre mooring ropes. *Applied Ocean Research*, vol. 112, pp. 102709, 2021.
[13] D. M. da Cruz, T. L. Popiolek Júnior, M. A. Barreto, C. E. M. Guilherme, and F. T. Stumpf. Evaluation of energy models for numerical simulation of the mechanical behavior of polyester multifilaments. *The Journal of Engineering and Exact Sciences*, vol. 9, n. 1, pp. 15321–01e, 2023a.
[14] F. T. Stumpf, C. E. M. Guilherme, D. M. da Cruz, da A. H. M. Fonseca Thomé da Silva, and M. B. Bastos. A general constitutive model for the numerical simulation of different synthetic fibres used in offshore mooring. *Ships and Offshore Structures*, vol. 18, n. 9, pp. 1338–1344, 2023.
[15] F. T. Stumpf, de Ávila M. Barreto, D. M. da Cruz, and C. E. M. Guilherme. Numerical simulation of multi-material hybrid lines for offshore mooring. *Ocean Engineering*, vol. 305, pp. 117979, 2024.
[16] D. M. da Cruz, T. L. Popiolek Júnior, M. A. Barreto, S. P. de Souza, L. B. Zangalli, A. J. da Cruz Júnior, T. C. Martins, A. L. N. da Silva, I. N. Bastos, and C. E. M. Guilherme. Numerical simulation with hyperelastic constitutive model for high-performance multifilaments used in offshore mooring ropes. *The Journal of Engineering and Exact Sciences*, vol. 10, n. 2, pp. 17255, 2024b.
[17] D. M. da Cruz, L. B. Zangalli, M. A. Barreto, I. N. Bastos, and A. L. N. da Silva. Numerical simulation of the stress-strain behavior of polyester subropes for offshore mooring and relationship with change stiffness during the test protocol. In *ROG.e 2024*, pp. 3215, Rio de Janeiro, Brasil, 2024c.
[18] D. M. da Cruz, L. B. Zangalli, M. A. Barreto, A. L. N. da Silva, and I. N. Bastos. Numerical simulation of creep behavior in low creep hmpe fibers used for offshore mooring ropes. In *Offshore Technology Conference Brasil*, pp. OTC–36033–MS, Rio de Janeiro, Brasil, 2025.
[19] D. M. da Cruz, A. Penaquioni, L. B. Zangalli, M. B. Bastos, I. N. Bastos, and A. L. N. da Silva. Non-destructive testing of high-tenacity polyester sub-ropes for mooring systems. *Applied Ocean Research*, vol. 134, pp. 103513, 2023b.
[20] International Organization for Standardization. *Textiles — Standard atmospheres for conditioning and testing*. International Organization for Standardization. ISO 139:2005, 2005.
[21] J. C. Simo and T. J. R. Hughes. *Computational Inelasticity*. Interdisciplinary Applied Mathematics. Springer Science & Business Media, New York, 7 edition, 2006.
[22] P. J. Flory. Thermodynamic relations for high elastic materials. *Transactions of the Faraday Society*, vol. 57, pp. 829–838, 1961.
[23] O. H. Yeoh. Some forms of the strain energy function for rubber. *Rubber Chemistry and Technology*, vol. 66, n. 5, pp. 754–771, 1993.